

A Modified Non-Stationary MIMO Channel Model Under 3D Scattering Scenarios

Qiuming Zhu^{1,2}, Kaili Jiang¹, Xiaomin Chen¹, Cheng-Xiang Wang², Xujun Hu¹ and Ying Yang¹

¹College of Electronic Information Engineering, Nanjing University of Aeronautics and Astronautics, Nanjing, 211100, China

² Institute of Sensors, Signals and Systems, School of Engineering & Physical Sciences, Heriot-Watt University, Edinburgh, UK

Email: zhuqiuming@nuaa.edu.cn, karry2780@163.com, chenxm402@nuaa.edu.cn, cheng-xiang.wang@hw.ac.uk, huxujun123@nuaa.edu.cn, yingy@nuaa.edu.cn

Abstract—Due to rapid movements of the transmitter and receiver, propagation channels of mobile communication systems show non-stationarity characteristics. A modified non-stationary multiple-input multiple-output (MIMO) channel model between the base station and mobile station under three dimensional (3D) scenarios is proposed. The new model takes the continuity of fading phase into account and guarantees more realistic Doppler frequencies. Meanwhile, extended 3D time evolving algorithms of channel parameters, including the path number based on birth-death processes of clusters, path delays, path powers, and angles of arrival and departure, are given and analyzed. Analytical and simulation results demonstrate that our channel model can characterize the properties of non-stationarity, and simulated results of time-variant autocorrelation function (ACF) and spatial cross-correlation function (CCF) are well consistent with the corresponding theoretical ones. The proposed channel model can be applied to performance evaluation and validation of the fifth generation (5G) wireless communication systems under time-variant scattering scenarios.

Index Terms—Non-stationary channel, 3D multiple-input multiple-output (MIMO) channel model, Doppler frequency, birth-death process, correlation function.

I. INTRODUCTION

MIMO technologies have drawn great research interests for their ability to improve spectral efficiency and link reliability significantly [1]. However, all these benefits can only be achieved with thoroughly understanding of the fading characteristics of the MIMO propagation channel. Most of existing models assume that channels satisfy the wide sense stationary (WSS) assumption [2]-[4]. However, measurement campaigns have shown that statistical properties of received signals are time-variant and channel fadings also have the characteristic of non-stationarity [5], [6]. Therefore, how to model non-stationary MIMO channels has been a hot research in the field of wireless communication [7]-[14].

Different approaches have been introduced in the recent literatures. Among them, non-stationary channel models originated from geometry-based stochastic models (GBSMs) attracted most attentions in the past a few years [7]-[12]. GBSMs also have formed the basis of most standard channel models, such as IMT-Advanced model [7] and WINNER+ model [8]. By incorporating the feature of

time evolution, several non-stationary GBSMs have been proposed in [9]-[12]. A non-stationary 2D model for HST channel can be found in [9]. The authors assumed that scatters were fixed in the form of multiple ellipses and updated the channel states by tracking the instantaneous position of mobile station (MS). An extend 3D model for V2V channel was proposed in [10], where authors used the two-sphere model to mimic moving vehicles and the multiple confocal elliptic-cylinder models to depict roadside environments. Moreover, a twin-cluster approach was adopted by [11] and [12]. This approach takes multi-bounced scatters into account and becomes more realistic.

It should be mentioned that aforementioned GBSM-based methods [9]-[12] model the non-stationary channel by dividing it into several segments, in which the WSS assumption is approximately satisfied and the original GBSMs with different parameters are applied. The main difference of these models is focused on the updating algorithms of time evolving channel parameters. However, we have found the generated channel fading phase with this procedure is discontinuous, which leads to the Doppler frequency shift does not agree well with the analytical one. A similar problem was reported in [13-14] very recently, when authors analyzed the v2v scenario with the mobile stations moving non-uniformly. These facts motivate us to develop an upgraded non-stationary channel model, which can overcome this shortcoming and becomes more accordant with the real world.

Overall, this paper proposes a modified non-stationary MIMO channel model under 3D scenarios. The new model takes the continuity of fading phase into account and guarantees more realistic Doppler frequency shift. Meanwhile, extended 3D time evolving algorithms of channel parameters, including the path number, path delays and path powers, are given. Moreover, the close form expressions of time-variant angles of arrival (AOA) and departure (AOD) both on the azimuth and elevation plane, are also derived.

The rest paper is organized as follows. In Section II, a modified non-stationary MIMO channel model between BS and MS under 3D scattering environment are introduced. Section III gives the corresponding updating algorithms of channel parameters. In Section IV, the theoretical ACF and CCF of our channel model are

analyzed. In addition, simulation results of ACF and CCF are also completed and validated. Finally, conclusions are shown in Section V.

II. MODIFIED NON-STATIONARY 3D MIMO CHANNEL MODEL

Let us consider a typical cellular channel model, which employs GBSM method to represent the propagation channel between BS and MS under 3D environments as illustrated in Fig.1. Let us assume that the BS and the MS are equipped with Q and P antenna elements, respectively. The sub-channel between each pair of antenna elements includes several propagation paths and each path is made of some clusters, where cluster A at the BS side denotes the first bounce and cluster Z at the MS side denotes the last bounce. The propagation environment between cluster A and Z can be abstracted as a virtual link [11]-[12].

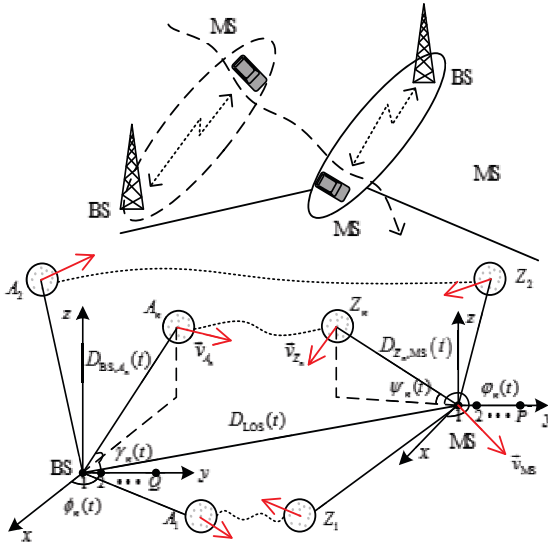


Fig. 1. MIMO channel model under a 3D environment.

The small scale-fading model for MIMO channel can be expressed as a complex matrix $\mathbf{H}(t, \tau) = [h_{qp}(t, \tau)]_{P \times Q}$ where each element $h_{qp}(t, \tau)$ denotes the complex channel impulse response (CIR) between BS antenna element $p(p=1, 2, \dots, P)$ and MS antenna element $q(q=1, 2, \dots, Q)$. In this paper, we assume that each sub-channel includes a line-of-sight (LOS) component and several non-line-of-sight (NLOS) components, which can be modeled as

$$\begin{aligned} h_{qp}(t, \tau) &= \sqrt{\frac{K}{K+1}} \cdot h_{qp}^{\text{LOS}}(t) \delta(\tau - \tau_{qp}^{\text{LOS}}(t)) \\ &+ \sum_{n=1}^{N(t)} \sqrt{\frac{P_n(t)}{K+1}} \cdot h_{qp,n}(t) \delta(\tau - \tau_{qp,n}(t)) \end{aligned} \quad (1)$$

where K is Rician factor, $N(t)$ is the number of NLOS paths, $\tau_{qp}^{\text{LOS}}(t), \sqrt{K/(K+1)}$ are the delay and the power of LOS path, and $\tau_{qp,n}(t), \sqrt{P_n(t)/(K+1)}$ are the delay and the power of the n th NLOS path.

For the LOS path, the CIR can be expressed as

$$h_{qp}^{\text{LOS}}(t) = e^{jk(\vec{s}_{\text{MS}}^{\text{LOS}}(t) \cdot \vec{r}_p)} e^{jk(\vec{s}_{\text{BS}}^{\text{LOS}}(t) \cdot \vec{r}_q)} e^{jk \int_0^t \vec{v}_{\text{MS}} \cdot \vec{s}_{\text{MS}}^{\text{LOS}}(t') dt'} e^{j\Phi^{\text{LOS}}} \quad (2)$$

where $k = 2\pi f_0/c_0$ denotes the wave number, f_0, c_0 represent the carrier frequency and the speed of light, $\vec{s}_{\text{MS}}^{\text{LOS}}(t), \vec{s}_{\text{BS}}^{\text{LOS}}(t)$ are the spherical unit vector of arrival and departure signal, \vec{r}_p, \vec{r}_q are the location vectors of the q th MS antenna and the p th BS antenna, respectively, \vec{v}_{MS} denotes the vector of MS velocity, and Φ^{LOS} is the random initial phase.

For NLOS components, the CIR can be expressed as

$$h_{qp,n}(t) = \sqrt{\frac{1}{M} \sum_{m=1}^M} e^{jk(\vec{s}_{\text{MS},n,m}^T(t) \cdot \vec{r}_p) + jk(\vec{s}_{\text{BS},n,m}^T(t) \cdot \vec{r}_q) + jk \int_0^t (\vec{v}_{Z_n, \text{MS}} \cdot \vec{s}_{\text{MS},n,m}(t')) dt'} \quad (3)$$

where M denotes the number of sub-paths (or rays), $\vec{s}_{\text{MS},n,m}^T(t), \vec{s}_{\text{BS},n,m}^T(t)$ are the spherical unit vector of m th ray within n th path arrival and departure signal, $\vec{v}_{Z_n, \text{MS}}$ is the relative velocity between MS and cluster Z_n , and $\Phi_{n,m}$ is the random initial phase.

It should be noticed that our non-stationary channel model turns to the classic stationary MIMO channel model [2]-[4], when all channel parameters keep unchanged over different time. In this case, the Doppler frequency shift of LOS path is also time-invariant, which is defined by

$$f^{\text{LOS}} = k \vec{v}_{\text{MS}} \cdot \vec{s}_{\text{MS}}^{\text{LOS}} / 2\pi. \quad (4)$$

The corresponding accumulated phase caused by Doppler frequency is continuous and equals to $2\pi f^{\text{LOS}} t$.

For non-stationary case, the Doppler frequency shift of LOS path should be time-variant and is denoted as $f^{\text{LOS}}(t)$. Most of conventional non-stationary channel models [9-12] use $2\pi f^{\text{LOS}}(t)t$ to represent the phase. However, it can be proved that the phase of this form is discontinuous, and the output Doppler frequency shift also does not equal to $f^{\text{LOS}}(t)$. A similar problem is happened as well to the NLOS components. To overcome this shortcoming, in our model we adopt $2\pi \int_0^t f^{\text{LOS}}(t') dt$ instead to calculate the accumulated phase, which can guarantee continuous fading phase.

III. UPDATING ALGORITHMS OF CHANNEL PARAMETERS

A. Time-varying distances

With the movements of MS and clusters, distances between MS, BS and clusters change over time. For simplicity, we assume all velocities keep constant and initial locations can be obtained by a measurement campaign or generation randomly. In Fig.1, all instantaneous locations at time instant $t + \Delta t$ can be obtained by following iterative algorithms,

$$\vec{L}_{\text{MS}}(t + \Delta t) = D_{\text{LOS}}(t) \cdot \vec{s}_{\text{BS}}^{\text{LOS}}(t) + \vec{v}_{\text{MS}} \cdot \Delta t \quad (5)$$

$$\vec{L}_{A_n}(t + \Delta t) = D_{\text{BS},A_n}(t) \cdot \vec{s}_{\text{BS},n}(t) + \vec{v}_{A_n} \cdot \Delta t \quad (6)$$

$$\vec{L}_{Z_n}(t + \Delta t) = \vec{L}_{\text{MS}}(t) + D_{Z_n, \text{MS}}(t) \cdot \vec{s}_{\text{MS},n}(t) + \vec{v}_{Z_n, \text{MS}} \cdot \Delta t \quad (7)$$

where $\vec{s}_{BS,n}(t), \vec{s}_{MS,n}(t)$ are the spherical unit vector of n th path arrival and departure signal, and \vec{v}_{A_n} denotes the movement vector of cluster A_n .

Based on time-variant locations of cluster A_n , cluster Z_n and MS, the corresponding distances between each other can be defined and calculated by

$$\begin{aligned} D_{BS,A_n}(t) &= \|\vec{L}_{A_n}(t)\| \\ D_{Z_n,MS}(t) &= \|\vec{L}_{Z_n}(t) - \vec{L}_{MS}(t)\| \\ D_{LOS}(t) &= \|\vec{L}_{MS}(t)\|. \end{aligned} \quad (8)$$

B. Time-variant path number, delays and powers

The number of NLOS paths is time varying, which means some paths can disappear (death) and some new paths can appear (birth). Let us set the birth and death rates as λ_G, λ_R , and model the time evolution of path number as a Markov process [11]. Thus, the survival probability of each path during time interval Δt can be calculated by

$$P_v(t) = e^{-\frac{\lambda_R(\delta_{MS} + \delta_{MC})}{D_c}} \quad (9)$$

where δ_{MS} and δ_{MC} are the channel fluctuations caused by movements of MS and clusters, where $\delta_{MS} = \|\vec{v}_{MS}\| \Delta t$, $\delta_{MC} = P_F (\|\vec{v}_{A_n}\| + \|\vec{v}_{Z_n}\|) \Delta t$, P_F is the percentage of moving clusters, D_c is the correlation distance.

The delay of n th path can be represented as

$$\tau_n(t) = [D_{BS,A_n}(t) + D_{Z_n,MS}(t)]/c_0 + \tilde{\tau}_n(t) \quad (10)$$

where $\tilde{\tau}_n(t)$ denotes the equivalent delay of virtual link, and can be updated by a first-order filtering method [12]

$$\tilde{\tau}_n(t) = \tilde{\tau}_n(t - \Delta t) e^{-\frac{\Delta t}{D_s}} + (1 - e^{-\frac{\Delta t}{D_s}}) X \quad (11)$$

where D_s denotes the decorrelation speed of time-variant delay which is determined by propagation environments, and $X \sim U(D_{LOS}(t), \tau_{max})$, τ_{max} denotes the maximum delay. After all path delays are obtained, we use the measurement-based method of WINNER+ model [8] to calculate the corresponding average power of each path,

$$\tilde{P}_n(t) = \exp\left(-\tau_n(t) \frac{(1 - r_\tau)}{r_\tau \sigma_\tau}\right) 10^{-\frac{Y_n}{10}} \quad (12)$$

where r_τ is the delay scalar, σ_τ is the delay spread, and Y_n follows the Gaussian distribution $N(0, 3)$.

C. Time-variant angles of departure and arrival

A time evolving method of angles under 2D environment has been studied in [11]. Here, we extend this idea to 3D scenarios, which include elevation plane and azimuth plane. Channel measurements have showed that the marginal distribution of power angular spectrum (PAS) in elevation is Laplacian, while the PAS in azimuth is truncated Gaussian [8].

In our model, the original angle sets of initialized paths

or new appeared paths are generated randomly according to the aforementioned PAS or obtained by a measurement campaign. During time evolving stage, we only track mean angles of AOA and AOD for simplicity. Based on geometrical relationships in Fig.1, the elevation angle of departure (EAOD) $\gamma_n(t)$ at time t can be expressed as

$$\gamma_n(t) = \arctan\left(\frac{D_{BS,A_n}(t_0) \sin \gamma_n(t_0)}{l_n(t)}\right) \quad (13)$$

where $l_n(t)$ denotes projective length of n th path from BS to cluster A_n , and can be calculated by

$$l_n(t) = \sqrt{\left(D_{BS,A_n}(t_0) \cos \gamma_n(t_0)\right)^2 + \left(\|\vec{v}_{A_n}\| t\right)^2} - \frac{2 D_{BS,A_n}(t_0) \|\vec{v}_{A_n}\| t \cos \gamma_n(t_0) \cos(\beta)}{2 D_{BS,A_n}(t_0) \|\vec{v}_{A_n}\| t \cos \gamma_n(t_0) \cos(\beta)}. \quad (14)$$

Moreover, β can be obtained by

$$\beta = \pi - (\phi_n(t_0) - \Psi_{A_n}), \quad \beta \in [0, \pi]. \quad (15)$$

Similarly, the updating algorithm for the azimuth angle of departure (AAOD) $\phi_n(t)$ can be expressed as

1) if $0 < \phi_n(t_0) \leq \pi$,

$$\phi_n(t) = \begin{cases} \phi_n(t_0) + \alpha_n(t), & \phi_n(t_0) < \Psi_{A_n} < \phi_n(t_0) + \pi \\ \phi_n(t_0) - \alpha_n(t), & \text{else} \end{cases}. \quad (16)$$

2) if $\pi < \phi_n(t_0) \leq 2\pi$

$$\phi_n(t) = \begin{cases} \phi_n(t_0) - \alpha_n(t), & \phi_n(t_0) - \pi < \Psi_{A_n} < \phi_n(t_0) \\ \phi_n(t_0) + \alpha_n(t), & \text{else} \end{cases}. \quad (17)$$

where $\alpha_n(t)$ denotes the angle of projection of n th path from BS to cluster A_n at time t_0 and t , which can be calculated by

$$\alpha_n(t) = \arccos \frac{(D_{BS,A_n}(t_0) \cos \gamma_n(t_0))^2 + l_n^2(t) - (\|\vec{v}_{A_n}\| t)^2}{2 D_{BS,A_n}(t_0) l_n(t) \cos \gamma_n(t_0)}. \quad (18)$$

For the case of AOA, we can obtain similar results with above procedures. In order to demonstrate time-variant properties of our channel model, we set simulation environment as C2-LOS scenario of WINNER+ model [8] and other simulation parameters are shown in Table I.

The time-variant power delay profiles (PDPs) based on our extended updating algorithms are shown in Fig. 2. In this figure, the total power is normalized and the y axis denotes the relative delay. As we can see, the power of each path decreases with the increase of relative delay, which also shows the trend of exponential decay in stochastic meaning. Meanwhile, the number of valid path changes over time, and the power of each survival path changes as well. To highlight the time evolving process, Fig. 3 gives AOD distributions at three time instants with the same simulation parameters. It is clearly showed that the angles of AOD change over time, which is caused by time-variant geometrical relationships.

TABLE I SIMULATION PARAMETERS

Definition	Value	Definition	Value
K	7dB	P_F	0.3
λ_G	0.8/m	λ_R	0.1/m
D_s	40m	τ_{\max}	220ns
r_r	2.5	σ_τ	41ns
$D_{\text{LOS}}(t_0)$	200m	f_0	2.4GHz
$D_{\text{BS},A_n}(t_0)$	25m	$\ \vec{v}_{\text{MS}}\ $	15m/s
$D_{Z_n,\text{MS}}(t_0)$	20m	$\ \vec{v}_{A_n}\ $	1.2m/s
$\phi_{\text{LOS}}(t_0)$	80°	$\ \vec{v}_{Z_n}\ $	1.5m/s
$\theta_{\text{LOS}}(t_0)$	6°	Ψ_{MS}	50°
$\phi_n(t_0), \gamma_n(t_0), \varphi_n(t_0), \psi_n(t_0), \Psi_{A_n}, \Psi_{Z_n,\text{MS}}$	random		

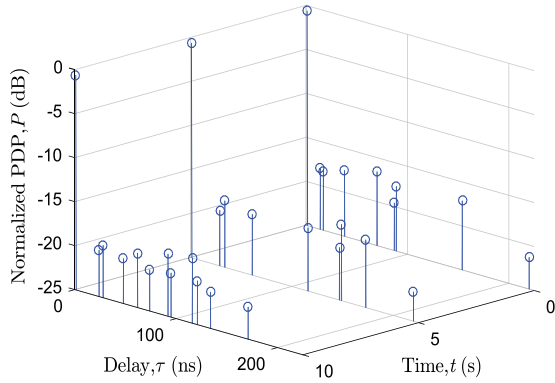


Fig.2. Time-variant PDPs under the C2-LOS scenario.

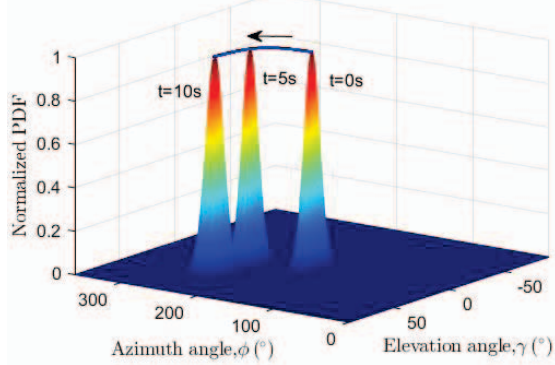


Fig. 3. Time-variant AODs under the C2-LOS scenario.

IV. NUMERICAL SIMULATION RESULTS

The channel transfer function (CTF) is defined as the Fourier transform of CIR [15], which is

$$H_{qp}(\vec{r}, f, t) = \int_{-\infty}^{\infty} h_{q,p}(t, \tau) e^{-j2\pi f \tau} d\tau \quad (19)$$

where \vec{r} denotes location vectors. In this paper, we assume the MIMO channel is non-stationary only on time domain. Under this assumption, the correlation between different frequencies is only related with the frequency lag

[16], and the correlation between different pairs of antenna elements only depends on the space lag. Thus, the 3D correlation function can be defined as

$$R_{q_1 p_1}^{q_2 p_2}(\Delta f, \Delta t; t) = E[H_{q_1 p_1}^*(f, t) H_{q_2 p_2}(f + \Delta f, t + \Delta t)] \quad (20)$$

Moreover, LOS and NLOS paths are usually uncorrelated, and thus (20) can be rewritten as

$$R_{q_1 p_1}^{q_2 p_2}(\Delta f, \Delta t; t) = R_{q_1 p_1}^{q_2 p_2, \text{LOS}}(\Delta f, \Delta t; t) + \sum_{n=1}^{N(t+\Delta t) \cap N(t)} R_{q_1 p_1, n}^{q_2 p_2, \text{NLOS}}(\Delta f, \Delta t; t) \quad (21)$$

where $N(t + \Delta t) \cap N(t)$ represents the set of shared paths. It should be mentioned that $R_{q_1 p_1, n}^{q_2 p_2, \text{NLOS}}(\Delta f, \Delta t; t)$ in (21) denotes the correlation function of one shared path, which also holds all correlation properties of NLOS paths in stochastic meaning.

For the case of ACF, the effect of survival probability from t to $t + \Delta t$ should be taken into account and the normalized ACF can be obtained by setting $q_i = q, p_i = p$ and $\Delta f = 0$, which is

$$\rho_{qp,n}(\Delta t; t) = \rho_{qp,n}^{\text{LOS}}(\Delta t; t) + \rho_{qp,n}^{\text{NLOS}}(\Delta t; t) \quad (22)$$

where

$$\begin{aligned} \rho_{qp,n}^{\text{LOS}}(\Delta t; t) &= R_{qp}^{\text{LOS}}(\Delta f = 0, \Delta t; t) \\ &= \frac{K}{K+1} h_{q,p}^{\text{LOS}*}(t) e^{j2\pi f \tau_{q,p}^{\text{LOS}}(t)} h_{q,p}^{\text{LOS}}(t + \Delta t) e^{-j2\pi f \tau_{q,p}^{\text{LOS}}(t + \Delta t)} \end{aligned} \quad (23)$$

and

$$\begin{aligned} \rho_{qp,n}^{\text{NLOS}}(\Delta t; t) &= \frac{R_{qp,n}^{\text{NLOS}}(\Delta f = 0, \Delta t; t)}{\sqrt{P_n(t)} \sqrt{P_n(t + \Delta t)}} \\ &= \frac{P_v(\Delta t) E[h_{q,p,n}^*(t) e^{j2\pi f \tau_{q,p,n}(t)} h_{q,p,n}(t + \Delta t) e^{-j2\pi f \tau_{q,p,n}(t + \Delta t)}]}{K+1} \end{aligned} \quad (24)$$

By setting $\Delta t = 0, \Delta f = 0$, we can obtain the normalized CCF between two different pairs of antenna elements as

$$\rho_{q_1 p_1, n}^{q_2 p_2}(\Delta t) = \rho_{q_1 p_1}^{q_2 p_2, \text{LOS}}(\Delta t) + \rho_{q_1 p_1, n}^{q_2 p_2, \text{NLOS}}(\Delta t) \quad (25)$$

where

$$\begin{aligned} \rho_{q_1 p_1}^{q_2 p_2, \text{LOS}}(\Delta t) &= R_{q_1 p_1}^{q_2 p_2, \text{LOS}}(\Delta f = 0, \Delta t = 0; t) \\ &= \frac{K}{K+1} h_{q_1, p_1, n}^*(t) e^{j2\pi f \tau_{q_1, p_1, n}(t)} h_{q_2, p_2, n}(t) e^{-j2\pi f \tau_{q_2, p_2, n}(t)} \end{aligned} \quad (26)$$

and

$$\begin{aligned} \rho_{q_1 p_1, n}^{q_2 p_2, \text{NLOS}}(\Delta t) &= \frac{R_{q_1 p_1, n}^{q_2 p_2, \text{NLOS}}(\Delta f = 0, \Delta t = 0; t)}{\sqrt{P_n(t)} \sqrt{P_n(t)}} \\ &= \frac{E[h_{q_1, p_1, n}^*(t) e^{j2\pi f \tau_{q_1, p_1, n}(t)} h_{q_2, p_2, n}(t) e^{-j2\pi f \tau_{q_2, p_2, n}(t)}]}{K+1} \end{aligned} \quad (27)$$

To verify correlation properties of our channel model, we set the scenario as C2-LOS [8] and the rest simulation

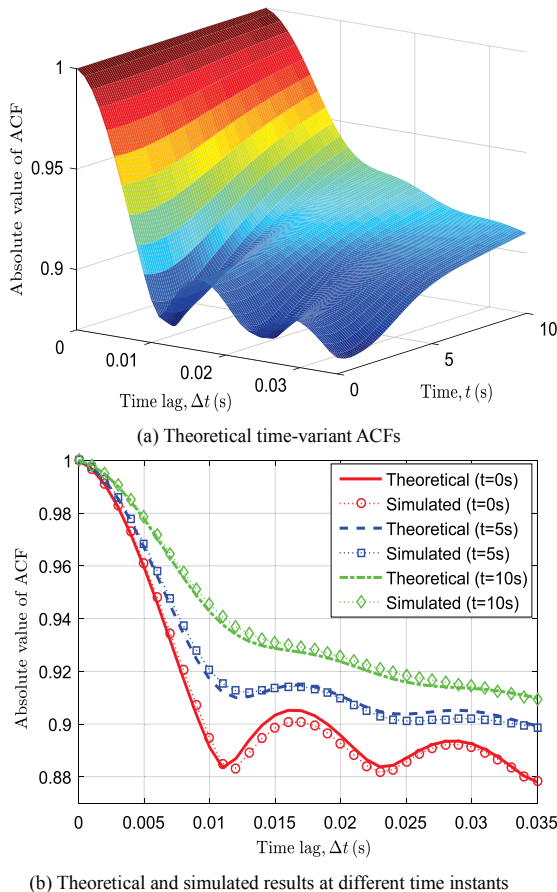


Fig. 4. Absolute values of ACFs under the C2-LOS scenario.

parameters as in Table I. Since the results of any path are similar, on following we only validate the first path. By using (22)-(24), theoretical ACFs caused by LOS path and the first NLOS path are calculated and given in Fig 4(a). It is obviously that the ACF changes over time due to time-variant channel parameters. The results of simulated ACFs at three time instants $t=0s$, $5s$ and $10s$ and corresponding theoretical ones are showed in Fig 4(b). It is showed that simulated results match analytical ones very well, which verifies the correctness of our theoretical derivations as well as simulations.

Under the same condition, by using (25)-(27), the theoretical CCFs are calculated and given in Fig. 5(a). In this figure, we assume antenna spaces on BS and MS are same, and the y axis has been normalized with respect to half wavelength. In addition, comparison between theoretical results and simulated ones at different time instants is presented in Fig. 5(b). The well agreement between theoretical and simulation results also demonstrates the correctness of channel model.

V. CONCLUSIONS

This paper has presented a modified non-stationary channel model for MIMO systems under 3D propagation scenarios, which can capture time-variant stochastic characters

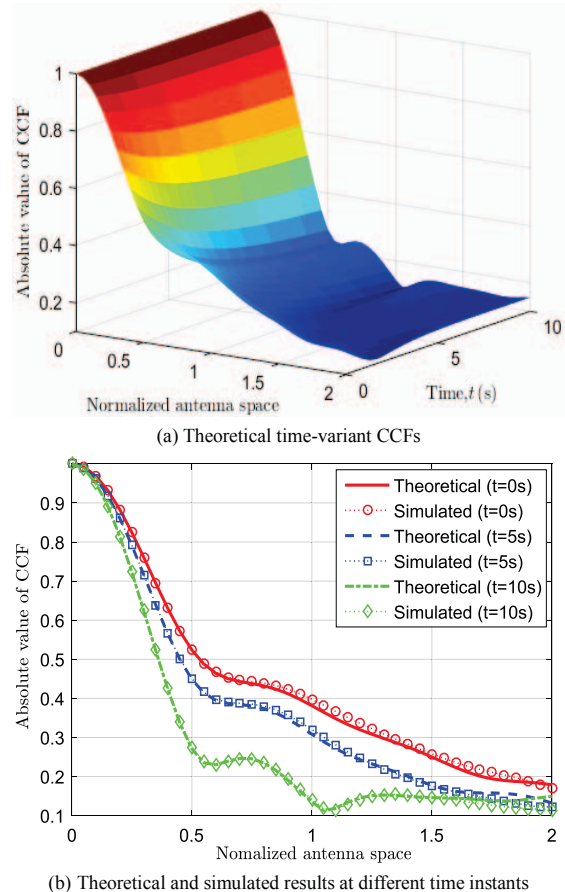


Fig. 5. Absolute values of CCFs under the C2-LOS scenario.

of small-scale fading due to the movements of the MS and clusters. The updating algorithms for time-variant channel parameters, such as the number of valid paths, delays, powers, and angles, have also been given and analyzed in details. Meanwhile, a universal correlation function of the non-stationary channel model, as well as two application cases of ACF and CCF, have been derived. Analytical and simulation results have shown that the proposed non-stationary channel model can guarantee continues fading phase and accurate Doppler frequency. In addition, stochastic properties such as ACF and CCF also agree well with the corresponding theoretical ones. Therefore, the new model can be applied to evaluate the state-of-the-art wireless systems under non-stationary environments in the future.

ACKNOWLEDGMENT

This work is supported by EU H2020 ITN 5G Wireless project (No. 641985), EU H2020 RISE TESTBED project (No. 734325), EU FP7 QUICK project (No. PIRSES-GA-2013-612652), EPSRC TOUCAN project (No. EP/L020009/1), Natural Science Foundation of China (No. 61210002), Fundamental Research Funds for the Central Universities (NS2015046, NS2016044), Foundation of Jiangsu Key Laboratory of Internet of

Things and Control Technologies (NJ20160027), Jiangsu Postdoctoral Foundation (1601017C), Open Foundation for Graduate Innovation Base of NUAA (KFJJ20160412, KFJJ20170405).

REFERENCES

- [1] M. Agiwal, A. Roy, and N. Saxena, "Next generation 5G wireless networks: A comprehensive survey," *IEEE Commun. Surv. Tut.*, vol. 18, no. 3, pp. 1617–1655, Feb. 2016.
- [2] A. Borhani and M. Patzold, "A unified disk scattering model and its angle-of-departure and time-of-arrival statistics," *IEEE Trans. Veh. Technol.*, vol. 62, no. 2, pp. 473–485, Feb. 2013.
- [3] T. J. Willink, "Wide-sense stationarity of mobile MIMO radio channels," *IEEE Trans. Veh. Technol.*, vol. 57, no. 2, pp. 704–714, Mar. 2008.
- [4] W. Weichselberger, M. Herdin, H. Ozcelik, and E. Bonek, "A stochastic MIMO channel model with joint correlation of both link ends," *IEEE Trans. Wireless Commun.*, vol. 5, no. 1, pp. 90–100, Jan. 2006.
- [5] B. Chen, Z. Zhong, and B. Ai, "Stationarity intervals of time-variant channel in high speed railway scenario," *China Commun.*, vol. 9, no. 8, pp. 64–70, Aug. 2012.
- [6] C.-X Wang, X. Cheng, and D. I. Laurenson, "Vehicle-to-vehicle channel modeling and measurements: recent advances and future challenges," *IEEE Commun.*, vol. 47, no. 11, pp. 96–103, ps/ Nov. 2009
- [7] ITU-R M.2135-1, "Guidelines for evaluation of radio interface technologies for IMT-Advanced," Geneva, Switzerland, Rep. ITU-R M.2135-1. Dec. 2009.
- [8] J. Meinila, P. Kyosti, L. Hentila, T. Jamsa, E. Suikkanen, E. Kunnari, and M. Narandzia, "D5.3: WINNER+ final channel models," CELTIC/CP5-026, June 2010.
- [9] A. Ghazal, C.-X Wang, B. Ai, D. Yuan, and H. Haas, "A nonstationary wideband MIMO channel model for high-mobility intelligent transportation systems," *IEEE Trans. Intell. Transp. Syst.*, vol. 16, no. 2, pp. 885–897, Apr. 2015.
- [10] Y. Yuan, C.-X Wang, and Y. He, "3D wideband non-stationary geometry-based stochastic models for non-isotropic MIMO vehicle-to-vehicle channels," *IEEE Trans. Wireless Commun.*, vol. 14, no. 12, pp. 6883–6895, July 2015.
- [11] A. Ghaza, Y. Yuan, and C.-X Wang, "A non-stationary IMT-A MIMO channel model for high-mobility wireless communication systems," *IEEE Trans. Wireless Commun.*, vol. 16, no. 4, pp. 2057–2068, Apr. 2017..
- [12] S. Wu, C.-X Wang, H. Aggoune, M. M. Alwakeel, and Y. He, "A non-stationary 3-D wideband twin-cluster model for 5G massive MIMO channels," *IEEE J. Sel. Areas Commun.*, vol. 32, no. 6, pp. 1207–1218, June 2014.
- [13] W. Dahech, M. Patzold, C. Gutierrez, and N. Youssef, "A non-stationary mobile-to-mobile channel model allowing for velocity and trajectory variations of the mobile stations," *IEEE Trans. Wireless Commun.*, vol. 16, no. 4, pp. 2057–2068, Apr. 2017
- [14] Q. Zhu, X. Liu, X. Yin, X. Chen, and C. Xue, "A novel simulator of non-stationary random MIMO channels in Rayleigh fading scenarios," *Int. J. Antenna. P.*, Aug. 2016
- [15] M. Patzold, *Mobile radio channels*, 2nd ed. West Sussex, U.K.: Wiley, 2012.
- [16] P. Bello, "Characterization of randomly time-variant linear channels," *IEEE Trans. Wireless Commun.*, vol. 11, no. 4, pp. 360–393, Dec. 1963.